AGU100 ADVANCING EARTH AND SPACE SCIENCE

JGR Atmospheres

RESEARCH ARTICLE
10.1029/2019JD030484

Key Points:
- WRF-Chem-parameterized wet scavenging scheme overestimates the removal of soluble trace gases
- Introducing an ice retention factor improves the parameterized wet-scavenging scheme simulation
- Model simulation is further improved with revised cloud-to-rain conversion parameters that are implemented at temperatures below freezing

Supporting Information:
- Supporting Information S1

Correspondence to:
Y. Li,
liyunyao@terpmail.umd.edu

Citation:
Li, Y., Pickering, K. E., Barth, M. C., Bela, M. M., Cummings, K. A., & Allen, D. J. (2019). Wet Scavenging in WRF-Chem Simulations of Parameterized Convection for a Severe Storm during the DC3 Field Campaign. *Journal of Geophysical Research: Atmospheres*, *124*, 7413–7428. https://doi.org/10.1029/2019JD030484

Received 15 FEB 2019
Accepted 3 JUN 2019
Accepted article online 18 JUN 2019
Published online 4 JUL 2019

Wet Scavenging in WRF-Chem Simulations of Parameterized Convection for a Severe Storm During the DC3 Field Campaign

Y. Li[1], K. E. Pickering[1], M. C. Barth[2], M. M. Bela[3], K. A. Cummings[4], and D. J. Allen[1]

[1]Department of Atmospheric and Oceanic Science, University of Maryland, College Park, MD, USA, [2]National Center for Atmospheric Research, Boulder, CO, USA, [3]Cooperative Institute for Research in Environmental Sciences (CIRES) at the NOAA Earth System Research Laboratory (ESRL) Chemical Sciences Division, University of Colorado, Boulder, Colorado, USA, [4]National Aeronautics and Space Administration (NASA), Kennedy Space Center, Orlando, FL, USA

Abstract Deep convection can transport surface moisture and pollution from the planetary boundary layer to the upper troposphere (UT) within a few minutes. The convective transport of precursors of both ozone and aerosols from the planetary boundary layer affects the concentrations of these constituents in the UT and can influence the Earth's radiation budget and climate. Some precursors of both ozone and aerosols are soluble and reactive in the aqueous phase. This study uses the Weather Research and Forecasting model coupled with Chemistry (WRF-Chem) to simulate the wet scavenging of precursors of both ozone and aerosols including CH_2O, CH_3OOH, H_2O_2, and SO_2 in a supercell system observed on 29 May 2012, during the 2012 Deep Convective Clouds and Chemistry (DC3) field campaign at cloud-parameterized resolution. The default WRF-Chem simulations underestimate the mixing ratios of soluble ozone precursors in the UT because the dissolved soluble trace gases are not released when the droplets freeze. In order to improve the model simulation of cloud-parameterized wet scavenging, we added ice retention factors for various species to the cloud-parameterized wet scavenging module and adjusted the conversion rate of cloud water to rainwater at temperatures below freezing in the cloud parameterization as well as in the subgrid-scale wet-scavenging calculation. The introduction of these model modifications greatly improved the model simulation of less soluble species.

1. Introduction

Deep convective storms can transport pollution and moisture from the planetary boundary layer (PBL) to upper troposphere (UT) in a few minutes (Chatfield & Crutzen, 1984; Dickerson et al., 1987; Skamarock et al., 2000). Transport of regional air pollutants from the PBL to the free troposphere by convection may transform regional boundary layer air pollution problems into global atmospheric chemistry issues (Kong & Qin, 1993, 1994; Lyons et al., 1986). Vertical transport of precursor gases of both ozone (O_3) and hydrogen oxides (HO_x, the sum of hydroxyl [HO] and hydroperoxy [HO_2] radicals) greatly enhances the production rate of O_3 in the UT cloud outflow (Pickering et al., 1990; Pickering, Scala, et al., 1992; Pickering, Thompson, et al., 1992) where the lifetime of O_3 is longer in comparison with the PBL region, which considerably impacts the Earth's radiation budget and climate (e.g., Lacis et al., 1990). Furthermore, the deep convective transport of surface moisture into the lower stratosphere increases the water vapor concentration (Homeyer et al., 2014), which is a prime driver for decadal climate change (Solomon et al., 2010).

The amount of O_3 and aerosol produced in the UT is dependent on the net transport by convection of gases that are soluble and reactive in the aqueous phase. In the UT, O_3 formation requires nitrogen oxides (NO_x, the sum of nitric oxide [NO] and nitrogen dioxide [NO_2]) and HO_x. The mechanism involves oxidation of NO by HO_2 and organic peroxy radicals (RO_2), followed by NO_2 photolysis and the combination of a resulting excited state O atom with an O_2 molecule. However, due to the short lifetime of HO_x, the amount of HO_x in the UT is determined by the abundance of longer-lived HO_x precursors such as hydrogen peroxide (H_2O_2), methyl hydroperoxide (CH_3OOH), and formaldehyde (CH_2O; Chatfield & Crutzen, 1984; Prather & Jacob, 1997), which are soluble and have aqueous phase chemical sources and sinks (Barth, Kim, Skamarock, et al., 2007; Carlton et al., 2007). H_2O_2 is produced by the reaction of the HO_2 radical with itself. CH_2O and CH_3OOH come from oxidation of methane and other hydrocarbons. The amount of NO_x in the

UT is dependent on its formation by lightning, the vertical transport of NO_x from the PBL, and the convective transport of the NO_x reservoir species nitric acid (HNO_3; Grassian, 2005), which is readily scavenged by cloud water and ice particles (Neu & Prather, 2012). NO_x is oxidized to HNO_3 in situ in the UT. NO_x in the UT has a longer lifetime and is more efficient in producing O_3 than at the surface. Furthermore, the formation of aerosols in the UT is affected by the deep convective transport of sulfur dioxide (SO_2), which is also soluble and a major source of sulfate aerosol in the UT.

The net deep convective transport of soluble species is governed by several physical processes within the convective core and anvil regions including dissolution in cloud water, removal by precipitation, and evaporation and release of dissolved gases. When droplets freeze, part of the dissolved gases may be released, and part retained in ice. Collectively, these processes are called wet scavenging. When wet scavenging occurs, the amount of trace gas that dissolves in cloud water is governed by Henry's law. The Henry's law coefficients vary greatly between species, with HNO_3 being extremely soluble and CH_3OOH being the least soluble among the species mentioned above.

Model simulations are often used to study wet scavenging. Crutzen and Gidel (1983) first included a simple treatment of wet scavenging into a two-dimensional model. Chameides (1984) introduced a time-dependent box model to analyze the coupled gas and aqueous-phase photochemistry of a stratiform cloud and found that the scavenging of atmospheric acidic gases and aerosols was an important source of acidity to cloud water. Lawrence and Crutzen (1998) included the gravitational settling of cirrus cloud particles and the gases trapped inside in the simulation. Mari et al. (2000) used a one-dimensional detraining/entraining plume model to investigate the vertical transport and wet scavenging of soluble gases in tropical deep convection. They found that small-scale, convective precipitation is effective in scavenging soluble gases, especially within convective updrafts. Pickering et al. (2001) used a two-dimensional cloud-resolving model to simulate the convective transport, wet scavenging, and lightning NO_x processes in the South Pacific Convergence Zone in the southwestern tropical Pacific during the 1999 Pacific Exploratory Mission Tropics B mission. Barth, Kim, Wang, et al. (2007) compared the trace gas mixing ratio results from eight cloud-resolving model simulations of an isolated storm sampled during the 1996 STERAO (Stratospheric-Tropospheric Experiment: Radiation, Aerosols, and Ozone) field campaign. They pointed out that substantial uncertainties existed in the scavenging efficiencies (SEs) of O_3 precursors such as H_2O_2, CH_2O, and HNO_3 that are soluble and/or reactive in cloud particles in the convective outflow region due to differing microphysics and assumptions about retention of chemical species during cloud drop freezing. For the cloud-parameterized scale, Neu and Prather (2012) describe an updated large-scale precipitation scavenging algorithm that has a more physical treatment of wet scavenging. The algorithm includes an improved calculation of wet removal in subgrid-scale cloudy and ambient environments as well as ice phase uptake of soluble species.

Wet scavenging is sensitive to the fraction of chemical species that are retained during cloud drop freezing; however, it is difficult to determine a reasonable value for each soluble species in the model. Furthermore, the observed ice retention fractions for individual species are highly variable. For example, Iribarne and Pyshnov (1990) estimated the retention fraction for H_2O_2 to be around 1, Snider and Jun (1998) obtained a value of 0.05, and von Blohn et al. (2011) found this value to be 0.64 ± 0.11. Moreover, highly soluble gases are more highly retained in ice than less-soluble species, as they can nearly completely dissociate in the liquid phase. For example, HNO_3 is completely retained (Iribarne & Pyshnov, 1990; von Blohn et al., 2011), while the observed retention fraction is 0.62 for SO_2 (Iribarne et al., 1990), which is less soluble than HNO_3. Jost et al. (2017) measured the retention coefficients of formaldehyde by wind tunnel experiments. The retention coefficients they obtained for CH_2O were 0.97 ± 0.11 and did not depend significantly on temperature or ventilation.

In May to June 2012, the Deep Convective Clouds and Chemistry (DC3) field campaign was conducted to examine the influence of midlatitude continental deep convective clouds on UT composition and chemistry, including determining the scavenging of soluble trace gases by thunderstorms. Fried et al. (2016) developed a method to calculate CH_2O SEs for the strong midlatitude convection that occurred during DC3. This method used nonreactive and insoluble organic tracers to determine the storm lateral entrainment, as well as storm inflow and outflow. The CH_2O SEs for different storms varied from 41% to 58%. Barth et al. (2016) analyzed the scavenging of H_2O_2 and CH_3OOH from six DC3 cases. The estimates of SEs were 79–97% for

H_2O_2 and 12–84% for CH_3OOH. Bela et al. (2016, 2018) conducted high-resolution cloud-resolved simulations with the Weather Research and Forecasting model coupled with Chemistry (WRF-Chem) model (Fast et al., 2006; Grell et al., 2005) to investigate the wet scavenging of soluble trace gases including H_2O_2, CH_3OOH, CH_2O, HNO_3, and SO_2 in storms measured during the DC3 field campaign. They found that the simulated SEs of all species, except HNO_3, are highly sensitive to the assumed values of the ice retention fractions. Their suggested ice retention fractions are 1.0 for CH_3OOH, 0–0.5 for CH_2O, and 0–0.25 for H_2O_2. Significant variations in SEs among storms and species were found in the simulated HNO_3 and SO_2, which precludes those measurements from constraining the ice retention fractions for these two species.

This study aims to evaluate and improve the subgrid-scale wet scavenging of trace gases in WRF-Chem. Unlike grid-scale wet scavenging that is calculated directly using predicted hydrometeors (e.g., cloud water, ice, rain, snow, and graupel), subgrid-scale wet scavenging is calculated using parameterized variables (e.g., updraft mass flux, downdraft mass flux, entrainment/detrainment rate, and precipitation rate) from the subgrid convection scheme. Grell and Freitas (2014) developed the subgrid-scale wet scavenging scheme used in WRF-Chem; however, this scheme does not include the process of dissolved gas release to the air when cloud droplets freeze, which leads to overremoval of the soluble trace gases in the UT. In this paper, WRF-Chem is employed at cloud-parameterized resolution to simulate a supercell thunderstorm that occurred during the DC3 field campaign. We will first evaluate the standard WRF-Chem subgrid-scale wet-scavenging scheme by comparing the simulation of a DC3 case study storm to observations. Then, we will add the retention of some species on frozen hydrometeors in the subgrid wet-scavenging module to improve model simulation of the soluble species. Finally, we modify the conversion ratio of cloud water to rain water in the subgrid-scale wet-scavenging scheme to further improve the model result. An overview of the case study storm can be found in section 2. The model setup details are provided in section 3. The discussion of the results and the improvement of the model are contained in section 4.

2. DC3 Case Study Storm

The case study storm was sampled during the 2012 DC3 field campaign, which was conducted from 15 May to 30 June. Storms were sampled in three locations: (1) northeastern Colorado, (2) central Oklahoma to west Texas, and (3) northern Alabama (Barth et al., 2015). The field campaign made use of numerous types of measurements to characterize the dynamical, physical, chemical, and lightning processes during and after active convection.

The case we chose is a multisupercell system that occurred in Oklahoma on 29 May. The observed radar reflectivity for this storm system from the NEXt generation weather RADar-Weather Surveillance Radar-1988 Doppler is shown in Figure 1. On 29 May, at ~2100 UTC a thunderstorm system with several convective updraft cores developed on the Oklahoma/Kansas border (Barth et al., 2015; DiGangi et al., 2016). Two isolated cells then initiated over northern Oklahoma and developed into a severe convective system with several updraft cores (Figure 1). Two extensively instrumented aircraft platforms, the National Aeronautics and Space Administration DC-8 and the National Science Foundation/National Center for Atmospheric Research Gulfstream-V (GV), started sampling the storm region at ~2000 UTC before convective initiation. The DC-8 aircraft measured the storm inflow from 2310 to 2315 UTC at 1.5-km height. At ~2330 UTC, the DC-8 spiraled up to sample the outflow on the eastern edge of the storm at ~10.8-km height (Figure 1). Meanwhile, the GV measured the storm outflow at ~11.7 km from 2359 to 0023 UTC (Fried et al., 2016). More details on storm evolution and structure are shown in DiGangi et al. (2016), Bela et al. (2016, 2018), and Li et al. (2017, 2018).

3. Model

The WRF-Chem V3.9 model containing the Advanced Research WRF dynamic core (Skamarock & Klemp, 2008) and coupled with atmospheric chemistry was employed at cloud-parameterized resolution (36 km) to simulate the deep convective transport and wet scavenging processes of five soluble species (CH_2O, CH_3OOH, H_2O_2, HNO_3, and SO_2) in the 29 May supercell case. The detailed model configuration and physics and chemistry options for this case are listed in Table 1. Model output was archived at 10-min intervals for use in this analysis.

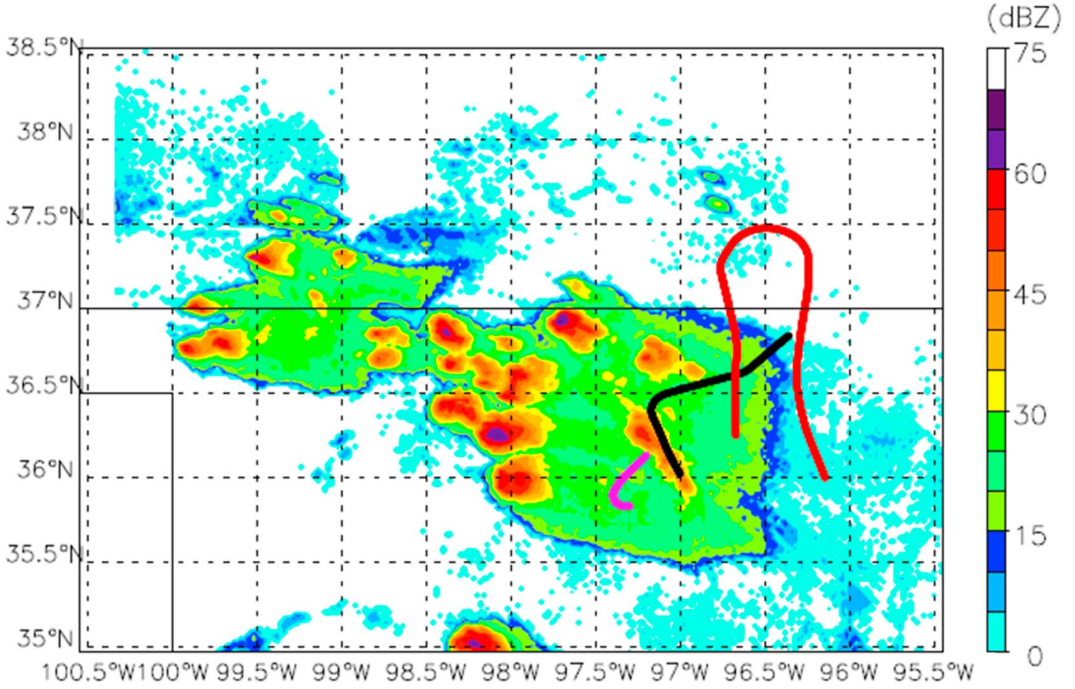

Figure 1. Column-maximum NEXt generation weather RADar radar reflectivity contours (dBZ) at 0000 UTC on 30 May. DC-8 inflow (magenta), DC-8 outflow (black), and Gulfstream-V outflow (red) sampling flight segments are shown by lines (*x* axis, longitude; *y* axis, latitude).

3.1. Meteorological Setup

The meteorological setup is discussed in Li et al. (2018), who focused on subgrid-scale convective transport in the same convective event. The simulation was initialized on 29 May at 1800 UTC using meteorological initial conditions (ICs) and boundary conditions (BCs) derived from the 6-hourly 12-km North American Mesoscale analysis. The model includes 90 vertical levels and has a 50-hPa model top. The time step for the simulation was 120 s. The Grell-Freitas (GF) cumulus scheme was used with the Kain-Fritsch (KF) closure. A detailed discussion of the GF scheme and the tuning of the closure options can be found in Li et al. (2018). The PBL option was the Mellor-Yamada-Janjic scheme (Janjić, 1994). The other main physics choices were the two-moment Morrison microphysics (Morrison et al., 2009) for cloud physics processes, the Rapid Radiative Transfer Model for General Circulation Models scheme (Iacono et al., 2008) for longwave and shortwave radiation, and the Noah scheme (Koren et al., 1999) for land surface processes.

3.2. Chemistry and Emission Options

The chemistry option was MOZART with GOCART aerosol chemistry using the Kinetic Preprocessor library (Pfister et al., 2011). Photolysis rates were calculated using the Fast-Tropospheric Ultraviolet-Visible (F-TUV) photolysis scheme (Tie et al., 2003). Fire emissions were calculated from the Fire Inventory from National Center for Atmospheric Research (Wiedinmyer et al., 2011) inventory. The 2011 U.S. Environmental Protection Agency's National Emission Inventory (NEI) data were used to create anthropogenic emissions. Anderson et al. (2014) and Travis et al. (2016) found that NEI overestimated the NO_x emission by 30–70%. Therefore, we reduced the NEI NO_x emission by 50% in our simulation. MEGAN v2.04 (Guenther et al., 2006) was used to generate biogenic emissions. Aircraft emission data were obtained from Baughcum et al. (1999).

We used the WRF-Chem default grid-scale wet-scavenging scheme, which is based on Neu and Prather (2012) and updated by Bela et al. (2016) to include ice retention factors in the grid-scale wet-scavenging scheme. In addition, subgrid convective transport, wet scavenging, and aqueous chemistry were turned on. More details about the subgrid convective transport scheme and subgrid wet-scavenging scheme are described in section 3.4. Lightning NO_x production is set at 82 moles per flash (Cummings, 2017) for both cloud-to-ground and intracloud flashes. More details on the lightning NO_x option are provided in section 3.5.

Table 1
WRF-Chem Model Configuration and Physics and Chemistry Options

Meteorology initial/boundary conditions	NAM 18 UTC
Chemistry initial/boundary conditions	MOZART scaled
Grid resolution	36 km
Vertical levels	90
Time step	120 s
Cumulus parameterization	GF with KF closure
Microphysics	Morrison
PBL	MYJ
Longwave radiation	RRTMG
Shortwave radiation	RRTMG
Lightning schemes	Price and Rind (1992; PR92) lightning flash rate scheme based on level of neutral buoyancy (Wong et al., 2013)
Cloud top height adjustment	0
Flashrate factor	17
LNO_x scheme	Combined intra-cloud and cloud-to-ground flashes single-mode vertical distributions with Lightning Mapping Array (LMA) flashes vertical profile
Moles of NO emitted per intracloud flash	82
Moles of NO emitted per cloud-to-ground flash	82
Fire emissions	FINN
Anthropogenic emissions	NEI with NO_x reduced by 50%
Biogenic emissions	MEGAN v2.04
Chemistry option	MOZCART
Grid-scale wet scavenging	Neu and Prather (2012) with the development from Bela et al. (2016) on ice retention factors
Subgrid-scale wet scavenging	on
Subgrid aqueous chemistry	on

Note. WRF-Chem = Weather Research and Forecasting model coupled with Chemistry; GF = Grell-Freitas; KF = Kain-Fritsch; PBL = planetary boundary layer; MYJ = Mellor-Yamada-Janjic; RRTMG = Rapid Radiative Transfer Model for General Circulation Models; FINN = Fire Inventory from National Center for Atmospheric Research; NEI = National Emission Inventory; MEGAN = Model of Emissions of Gases and Aerosols from Nature; MOZCART = MOZART with GOCART aerosol.

3.3. IC and BC for Chemistry

We used output from the global chemistry transport model MOZART-4 to create the chemical IC and BC. In order to better represent simulated inflow, we adjusted the IC to better match the vertical profile of aircraft observations using the equations listed in Table 2. The adjusted model low-level inflow trace gas mixing ratios are compared with aircraft data in Table 2. The differences between the adjusted simulation and observation of all the species in low-level inflow were within 10% of the aircraft measurements, except for H_2O_2. However, the overestimate of H_2O_2 in the inflow will not affect the H_2O_2 in the outflow due to its high solubility and short lifetime in the lower troposphere.

3.4. Subgrid Convective Transport and Wet Scavenging of Trace Gases

We used the subgrid convective transport scheme developed in Li et al. (2018). In this scheme, subgrid convective transport of trace gases was moved from the chemistry to physics module. Mass flux-related variables (i.e., entrainment and detrainment rate, cloud top height, cloud-base mass flux, downdraft mass flux, updraft mass flux, the originating level of updraft and downdraft, level of free convection, evaporation, and precipitation) from the GF cumulus parameterization were used to compute the subgrid convective transport of trace gases using the following equation (Grell & Freitas, 2014):

$$\left(\frac{\partial C}{\partial t}\right)_{\text{subgrid}} = -\frac{1}{\rho}\frac{\partial}{\partial z}\left[m_u(C_u-C_e)-m_d(C_d-C_e)+m_uC_{aq}\right]-\overline{C_{\text{si}}}+\overline{C_{so}}, \tag{1}$$

where C denotes the mass mixing ratio of a trace gas, ρ denotes air density, and m denotes mass flux. The subscripts e, u, and d denote the environment, updraft, and downdraft, respectively. C_{aq} denotes the chemical constituent in the aqueous phase. C_{so} (source) is calculated using an aqueous-phase chemistry routine.

Table 2
IC Formulation Equations Used to Adjust the Simulated Species at 1.5-km Altitude Closer to the DC8 Inflow Observations

Species	IC equations	Observation	Modified WRF-Chem inflow
CO	$C=C(72+2H)/100\ 0<H<14$ km	136.8 ± 1.1	141.4 ± 1.4
CH_2O	$C=C((14-H)*0.8+1)\ 0<H<14$ km	5.2 ± 0.3	4.9 ± 0.2
CH_3OOH	$C=C((14-H)*0.25+1)\ 0<H<14$ km	1.6 ± 0.1	1.6 ± 0.0
HNO_3	$C=C(58+3H)/100\ 0<H<14$ km	0.6 ± 0.1	0.6 ± 0.0
O_3	$C=C(60+10H)/100\ 0<H<4$ km	54.9 ± 1.9	59.5 ± 0.8
H_2O_2	$C=0.3C$	2.5 ± 0.2	6.6 ± 0.0
SO_2	—	—	0.5 ± 0.2

Note. WRF-Chem = Weather Research and Forecasting model coupled with Chemistry; IC = initial condition.

C_{si} (sink) is dependent on the conversion rate of cloud water to rain water and the solubility of the tracer and is computed in the subgrid wet-scavenging routine:

$$C_{si} = \alpha C_u\, m_u q_r, \tag{2}$$

where C_u represents the trace gas mixing ratio in the updraft, m_u represents the updraft air mass flux, and q_r represents the mass mixing ratio of rain. The variable α is calculated using a formula based on Henry's law. Details are shown in Text S1 and Table S1 in the supporting information. The effective Henry's law coefficients for soluble species are taken from Neu and Prather (2012) and Bela et al. (2016) with their variation with temperature shown in Table S2. The GF convective parameterization does not include ice physics. Therefore, the default subgrid wet-scavenging scheme assumes that all dissolved trace gases remain within the hydrometeors when temperature is below the freezing points.

3.5. Lightning NO_x (LNO_x) Option

The lightning option is PR92 (Price & Rind, 1992; Wong et al., 2013), which is used for predicting lightning flash rate for parameterized convection in WRF-Chem. The PR92 option uses cloud height to determine lightning flash rate. The cloud heights used in this scheme are based on the level of neutral buoyancy from the convective parameterization. The LNO_x scheme is based on Ott et al., 2009). Vertical profiles of flash channel lengths (Cummings, 2017) observed by the Oklahoma Lightning Mapping Array for the 29 and 30 May storm were used to distribute the simulated total flashes as well as the LNO_x production in the vertical. The peak of the 29 and 30 May flash channel distribution is at 10 km, which is 3 km higher than the default WRF-Chem distribution (Figure 2). The LNO_x production rate of 82 moles per flash is based on Cummings (2017). Thus, in our simulation, the LNO_x peak would be at higher altitude than in a default WRF-Chem simulation. LNO_x affects UT ozone production. Thus, a good simulation of LNO_x is very important for downwind ozone simulation. When comparing the simulated and observed NO_x peaks in the anvil region, we found that the amplitude was the same as observed; however, the height of the simulated peak was 0.5 km lower. The underestimate of the height resulted from the lack of proper consideration of LNO_x transport in the subgrid-scale convective transport module. In the subgrid-scale convective transport module, the trace gas mixing ratios in the updraft depend on the trace gas mixing ratios at the updraft initiation level and the entrainment/detrainment rate at each level above. There is little LNO_x at the updraft initiation level, and in the UT, the entrainment rate is very small. Therefore, the grid-scale LNO_x in the UT only has a small impact on the subgrid-scale NO_x convective transport in the parameterized updraft. In our future work, we plan to add a subgrid-scale LNO_x transport module in the model, to improve the NO_x simulation in the UT. In this paper, the underestimate of the subgrid-scale convective transport of LNO_x will have very little impact on the results and discussion of CH_2O, CH_3OOH, H_2O_2, and SO_2 (Barth et al., 2016) but will influence the results for HNO_3. Thus, we do not include discussion of HNO_3 in this paper.

4. Simulation Results and Model Improvements

4.1. Precipitation Simulation

We tried several different cumulus schemes to simulate the case study storm (Li et al., 2018). Compared to the National Centers for Environmental Prediction (NCEP) stage IV precipitation observations, we found

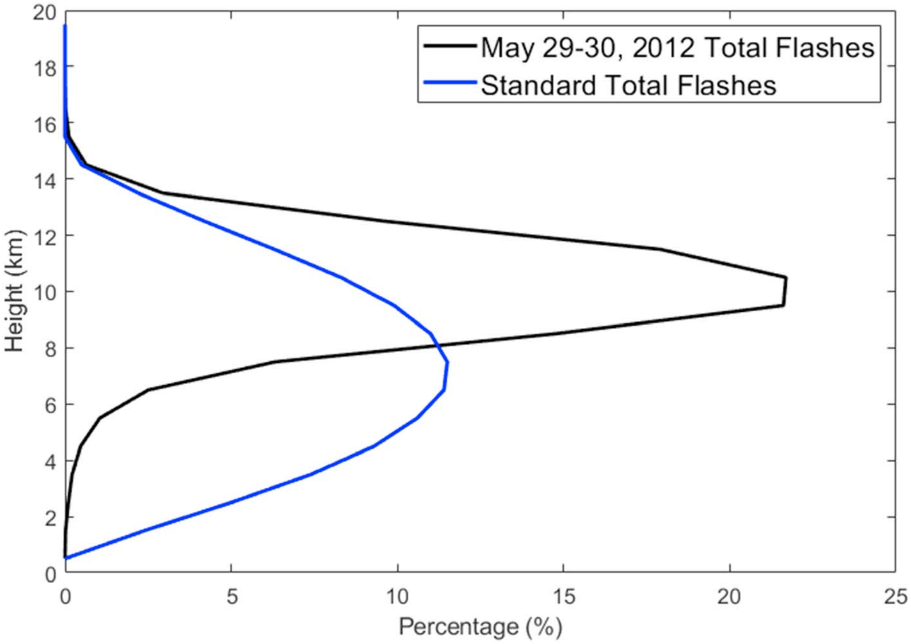

Figure 2. Vertical profile of percentage amounts of total flash channel lengths assigned to 1-km layers for Weather Research and Forecasting model coupled with Chemistry standard version (blue), and our revised version based on the 29 and 30 May 2012 Deep Convective Clouds and Chemistry storm (black).

that only the simulation with the GF cumulus scheme reproduces the location and extent of the storm precipitation region. The 3-hr precipitation simulation with the GF scheme matched the NCEP stage IV precipitation observations, while the hourly maximum precipitation at the aircraft measuring time was ~36.5% lower than the NCEP stage IV precipitation observation. In order to improve the simulated hourly precipitation, we tuned the closure options inside the GF scheme following Qiao and Liang (2015, 2016, 2017). The default GF scheme uses an average cloud-base mass flux from the results of four different closures, as discussed in Li et al. (2018). In Li et al. (2018), we reran the WRF simulation turning on one closure each time. We found that the simulation with the KF closure reproduced the maximum hourly precipitation to within 5% (Li et al., 2018, their Table 3). This closure scheme calculated the cloud-base mass flux based on the assumption that Convective Available Potential Energy is removed by convection over a specific time period. Our following analysis is based on this simulation (GF-KF).

The model with GF cumulus parameterization with KF closure (GF-KF run) produced a storm that began 80 min later than the observations. Therefore, observed 3-hr precipitation ending at 0000 UTC 30 May will be compared to modeled precipitation ending at 0120 UTC 30 May (Figures 3a–3d). The WRF-Chem simulations capture the storm location, precipitation strength, and the two-cell structure of the storm. Comparison of the lower two panels (Figures 3c and 3d) indicates that the precipitation for the 36-km resolution simulation is mainly subgrid scale; that is, the subgrid-scale mean precipitation is 2.8 times greater than the grid-scale mean precipitation. Therefore, the subgrid-scale convection dominates in this simulation.

4.2. Results With the Default Subgrid Convective Transport Scheme

Two initial WRF-Chem runs were conducted in our analysis of wet scavenging in the 29 May storm. In the first run, we ran WRF-Chem without wet scavenging (both grid and subgrid). In the second run, we ran with the WRF-Chem default wet-scavenging schemes (both grid and subgrid). We compared the simulated UT vertical profiles of in-cloud CH_2O, CH_3OOH, H_2O_2, and SO_2 along the aircraft tracks with the GV and DC8 outflow measurements. Results are shown in Figure 4. The WRF-Chem default wet-scavenging scheme removed too much CH_2O, CH_3OOH, and H_2O_2 with UT model concentrations being 98%, 80%, and 30% lower than observations, respectively. The simulated SO_2 was close to observation. The contribution of

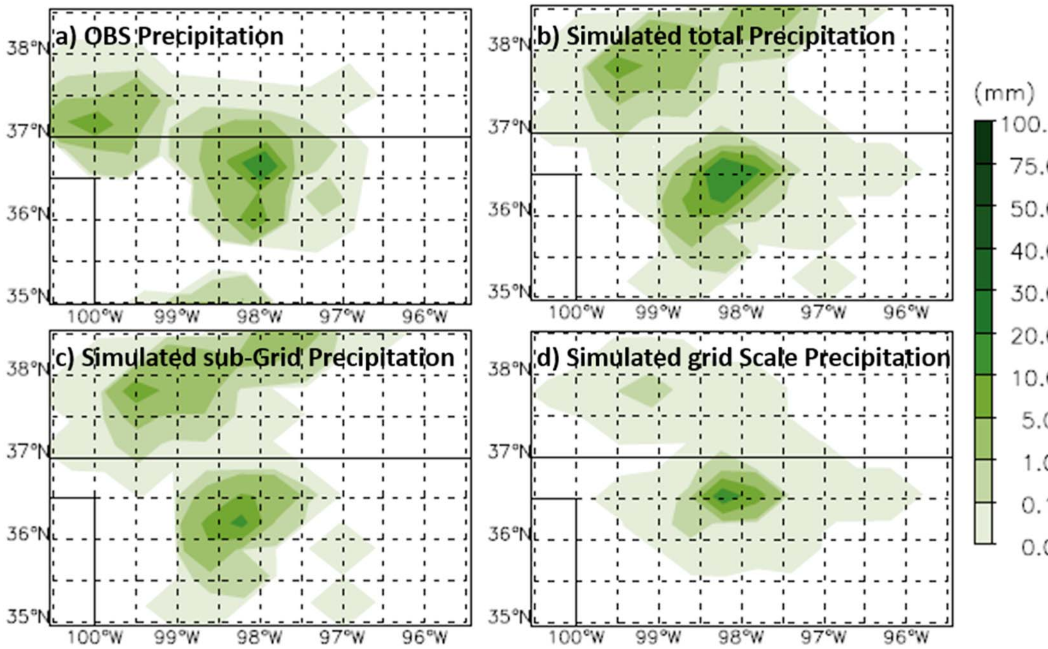

Figure 3. Three-hour precipitation observations (mm) averaged to model grid (a) at 0000 UTC on 30 May 2012; Weather Research and Forecasting model coupled with Chemistry simulated total precipitation (b), subgrid scale (c), and grid-scale precipitation (d) at 0120 UTC on 30 May 2012 (*x* axis, longitude; *y* axis, latitude). Note that the simulated storm started 80 min later than the observed real storm.

subgrid wet scavenging to the total wet scavenging is 57% for CH_2O, 51% for CH_3OOH, 10% for H_2O_2, and 72% for SO_2.

According to Grell and Freitas (2014), the subgrid-scale wet scavenging depends on the solubility of the tracer and on the conversion rate of cloud water to rain water. In order to improve the subgrid wet-scavenging simulation, we adjusted the solubility of the tracer by introducing an ice retention factor in section 4.3 and adjusted the conversion rate of cloud water to rain water in section 4.4.

4.3. Estimates of Retention on Ice

Bela et al. (2016) introduced ice retention factors to the WRF-Chem grid-scale wet scavenging module. Barth et al. (2016) and Bela et al. (2016) found that the SE of soluble trace gases were highly dependent on the ice retention factor during cloud drop freezing, suggesting ice physics impacts the wet-scavenging process. Their suggested ice retention fractions are 1.0 for CH_3OOH, 0-0.5 for CH_2O, and 0-0.25 for H_2O_2 for the 29 May 2012 storm.

One possible reason for the overestimation of subgrid wet scavenging in the UT is that the default WRF-Chem subgrid wet-scavenging scheme does not separate scavenging by ice and water. In the default model, there is no simulation of ice physics in the cumulus parameterization. In the default subgrid wet-scavenging scheme (Grell & Freitas, 2014), the hydrometeors at temperatures below 273.15 K are treated as cloud liquid water. Therefore, soluble species remain completely in the cloud water when hydrometeors exist above the freezing level of the cloud. However, in reality the scavenging processes are different before and after the cloud water freezes. When cloud water freezes, part of the dissolved gases may be released into the air and unavailable for wet scavenging (Barth et al., 2001; Barth, Kim, Wang, et al., 2007; Leriche et al., 2013). Therefore, wet scavenging will overestimate the SE if the ice, and liquid water processes are not handled separately.

Following Bela et al. (2016), we introduce an ice retention factor to the grid points with a temperature below 273.15 K to improve the model simulation of the subgrid wet-scavenging process. We assume that when the temperature is below the freezing point, a fraction, *r*, of the total dissolved gases stays in the cloud droplets, while (1-*r*) of the dissolved gases releases to the ambient air. This changes C_{si} in equation (2) to

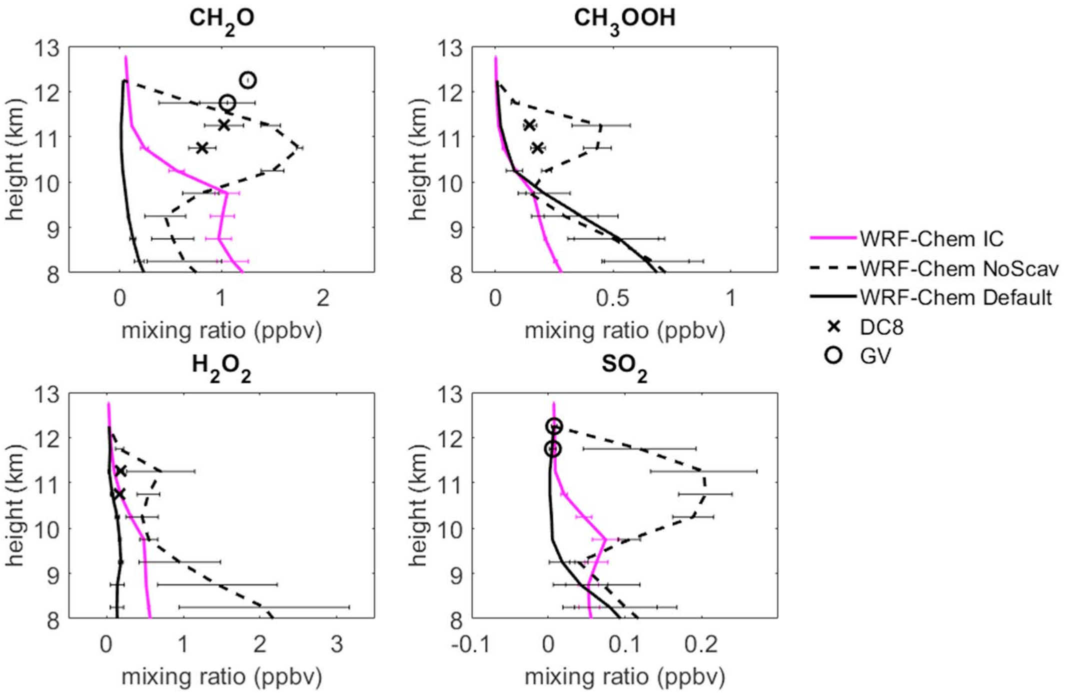

Figure 4. Mean outflow vertical profiles (ppbv) of CH_2O, CH_3OOH, H_2O_2, and SO_2, from the 29 May supercell storm as observed by the DC-8 (black cross) and Gulfstream-V (GV; black circle) aircraft, mean profiles as simulated in the 36-km default Weather Research and Forecasting model coupled with Chemistry (WRF-Chem) with (black solid line) and without (black dash line) parameterized wet scavenging. The simulations are compared with the initial conditions (ICs) for the cloud-parameterized run (magenta). Model profiles are shifted 0.75° west with respect to the aircraft profiles ensure sampling of model outflow.

$$C_{si} = \begin{cases} C_{si} & T \geq 273.15\text{ K} \\ rC_{si} & T < 273.15\text{ K} \end{cases}, \qquad (3)$$

where r is the ice retention factor. We tested five ice retention factor values (see Table 3): $r = 0$, $r = 0.1$, $r = 0.25$, $r = 1$ (same as the default scheme), and $r =$ var (values varying by species, as defined in Leriche et al., 2013). The ice retention factor was applied to both subgrid- and grid-scale wet scavenging.

The introduction of the ice retention factor reduced scavenging resulting in better agreement with measurements (Figure 5). Compared to the default WRF-Chem results ($r = 1.0$), when using $r = 0$, the differences between observation and simulation were reduced by 24%, 87%, and 77% for CH_2O, CH_3OOH, and H_2O_2. We compared the mean of the model simulation along the aircraft tracks between 10.75-11.75 km for DC8 and 11.75-12.25 km for GV in the storm outflow region with the mean of these aircraft measurements in Table 4. According to Li et al. (2018, their Figure 10), the model-simulated maximum detrainment layer was around 0.5 km lower than the observed layer, so in Table 4, we compare the aircraft measurement with a simulation model layer that is 0.5 km lower than the aircraft measuring height. For CH_2O, all the runs with wet scavenging underestimate the UT CH_2O mixing ratio and have larger biases than the run without wet scavenging. One possible reason is that the model removes too much CH_2O below the altitude of the freezing point. This is consistent with the cloud-resolved grid-scale wet-scavenging results of Bela et al. (2018) who found that most CH_2O scavenging occurs below the freezing level. When using subgrid-scale wet scavenging, the usage of $r = 0$ produced the closest result to the observation. For CH_3OOH and H_2O_2, $r = 0$ produced the best result with differences between observations and simulations less than 10% for CH_3OOH and 15% for H_2O_2. Similar to CH_2O, all

Table 3
Ice Retention Fraction Values for Each Soluble Species in the WRF-Chem Simulation

	CH_2O	CH_3OOH	H_2O_2	SO_2
No scav.	0	0	0	0
scav. r=0	0	0	0	0
scav. r=0.1	0.1	0.1	0.1	0.1
scav. r=0.25	0.25	0.25	0.25	0.25
scav. r=1	1	1	1	1
scav. r=var	0.64	0.02	0.64	0.02

Note. WRF-Chem = Weather Research and Forecasting model coupled with Chemistry.

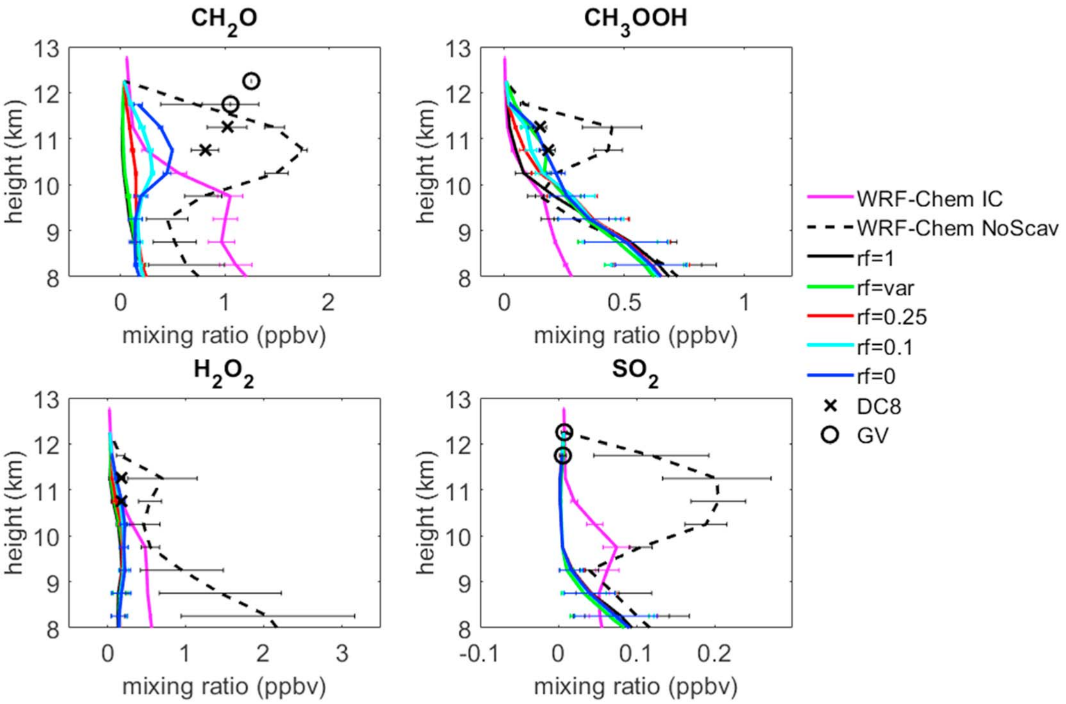

Figure 5. Similar to Figure 4, but for five sensitivity runs with different ice retention factors: r=0 (blue), r=0.1 (cyan), r=0.25 (red), r=var (green), and r=1.

the runs with wet-scavenging underestimate the UT CH_3OOH and H_2O_2 mixing ratio. For SO_2, all the runs with wet scavenging produced much better results than the no wet scavenging run.

Finally, we calculated SE for various trace gases from the WRF-Chem simulations using the following equation (Bela et al., 2016):

$$\mathrm{SE}(\%) = 100\times\left(\frac{\overline{C_{\mathrm{noscav}}}-\overline{C_{\mathrm{scav}}}}{\overline{C_{\mathrm{noscav}}}}\right), \tag{4}$$

where C_{noscav} and C_{scav} are the mean in-cloud outflow values of trace gases in the simulation without wet scavenging and the simulation with wet scavenging, respectively. The SE results are compared to the observed SE result from Bela et al. (2016) for the 29 May supercell case in Figure 6.

For CH_2O, all the runs overestimate the SE. However, lowering the ice retention factor reduces the difference between modeled and observed SEs, and the SE for the simulation with r = 0 is the closest one to the observation. For CH_3OOH, r = 0.25 produced the best result. For H_2O_2, the best result comes from the r=var (0.64) run. The best estimates of r for H_2O_2 and CH_3OOH from the SE analysis are larger than the estimates of r obtained by comparing the simulated and observed H_2O_2 and CH_3OOH mixing ratio. As we mentioned above, this is because the model overestimates the wet scavenging at locations where the temperature is above freezing. Thus, in order to match observations, the wet scavenging above the freezing level must be decreased. For SO_2, observations vary widely and provide no constraints on simulated SEs. Comparing the SEs for all the five species, we find that the simulated SEs for CH_3OOH are highly sensitive to the ice retention factor (for r ranging from 0 to 1, SE = 54–86%), which is consistent with Bela et al. (2018).

Table 4
Values From Observations and WRF-Chem Simulations of Mean Mixing Ratio (ppb) of Soluble Species in UT Outflow Region as a Function of Ice Retention Factor (r)

	Observation	r=0	r=0.1	r=0.25	r=var	r=1	No scav.
CH_2O	1.036	0.272	0.156	0.074	0.027	0.025	0.999
CH_3OOH	0.165	0.149	0.103	0.067	0.142	0.036	0.441
H_2O_2	0.175	0.147	0.128	0.086	0.066	0.053	0.624
SO_2	0.007	0.004	0.004	0.004	0.005	0.004	0.133

Note. WRF-Chem = Weather Research and Forecasting model coupled with Chemistry; UT = upper troposphere.

4.4. Improving the Cloud-to-Rain Ratio

The conversion ratio of cloud water to rain water also affects the mixing ratio of soluble species in the UT. The trace gases that are dissolved in

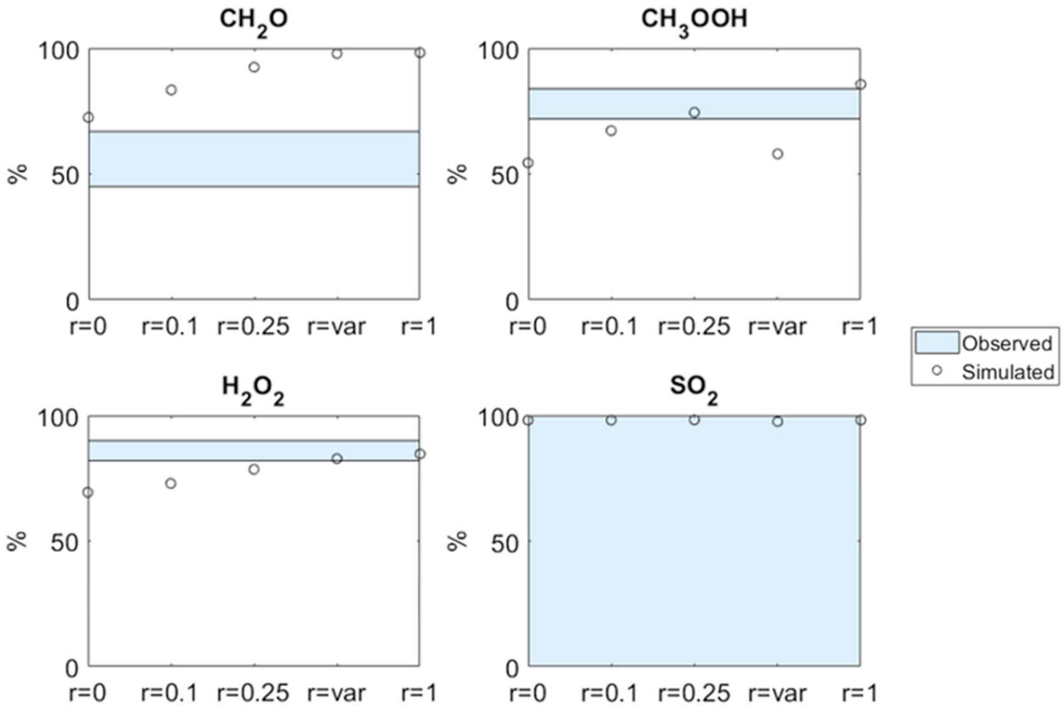

Figure 6. Observed scavenging efficiencies (shaded) and model-simulated scavenging efficiencies (circle) from five sensitivity runs with different ice retention factors: *r*=0, *r*=0.1, *r*=0.25, *r*=1, and *r*=var.

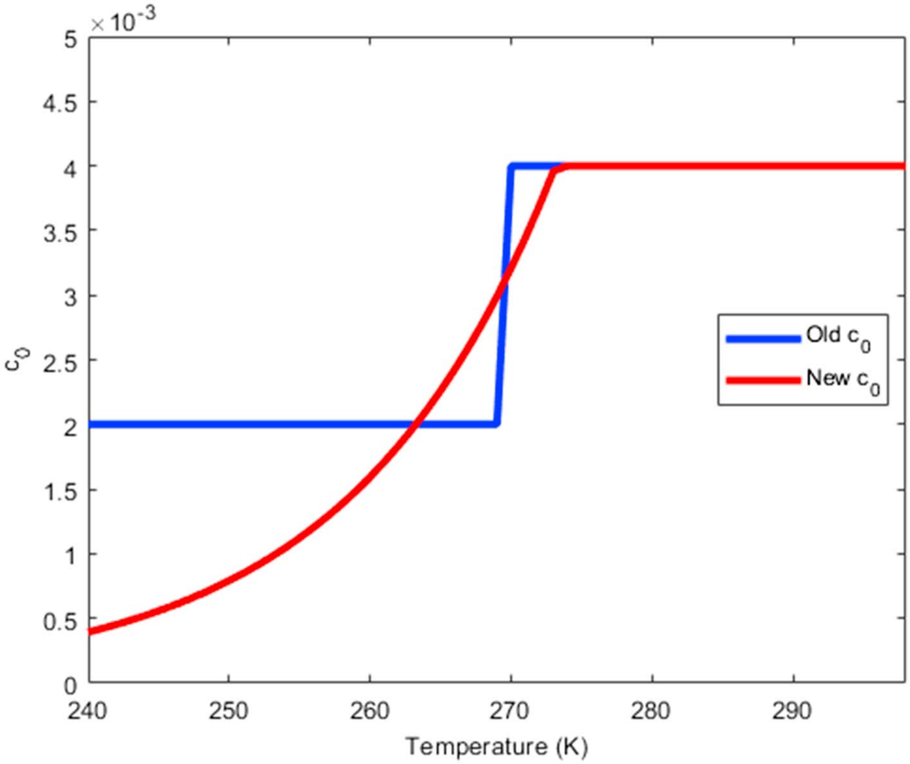

Figure 7. Conversion rate (c_0) of cloud water to rain water from the default Grell-Freitas scheme (blue) and the new conversion rate (red) based on Han et al. (2016).

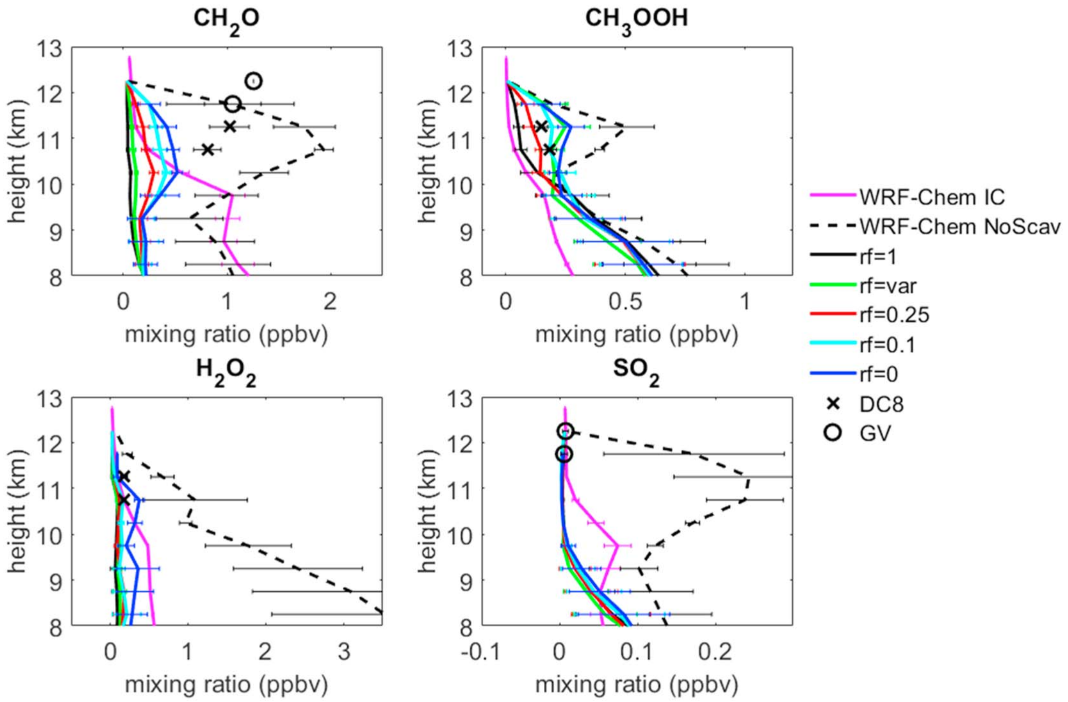

Figure 8. Similar to Figure 5, but for the WRF-Chem runs with the new conversion rate of cloud water to rain water.

the rain water are removed from the cloud by precipitation. Therefore, if the conversion ratio of cloud water to rain water is too large, the model could overestimate the removal of the soluble species. In the default GF cumulus scheme, the following equations are used to calculate the conversion rate ($c_{0,}$ m^{-1}) of cloud water to rain water:

$$c_0 = \begin{cases} 0.004 & T \geq 270\ \mathrm{K} \\ 0.002 & T < 270\ \mathrm{K} \end{cases}. \tag{5}$$

Han et al. (2016) proposed a revised conversion rate of cloud water to rain water based on a cloud-resolving simulation of a thunderstorm (Lim, 2011). They found that the conversion rate of cloud water to rain water decreases exponentially with height above the freezing level. Thus, in their modified scheme, the conversion rate (c_0) varies exponentially with temperature for below freezing temperatures. We adjusted the conversion rate following their method using the equation below:

$$c_0 = \begin{cases} 0.004 & T \geq 273.15\ \mathrm{K} \\ 0.004e^{[a(T-273.15)]} & T < 273.15\ \mathrm{K} \end{cases}, \tag{6}$$

where $a = 0.07$. The c_0 values between 220 and 298 K are shown in Figure 7. Compared to the default c_0 value in the GF scheme, the new c_0 is reduced below 260 K, which is at 6 km and above in the 29 May storm. The new conversion rate of cloud water to rain water was applied to both the subgrid-scale wet-scavenging module and the cumulus parameterization to maintain consistency. By using the new conversion rate, the precipitation was reduced by ~3%, and the mixing ratio of CO, an example of insoluble species, was increased by ~3% in the UT.

Table 5
Similar to Table 4, but for the Runs With the New Conversion Rate of Cloud Water to Rain Water

	OBS	r=0	r=0.1	r=0.25	r=var	r=1	No scav.
CH_2O	1.036	0.297	0.240	0.142	0.069	0.041	1.188
CH_3OOH	0.209	0.254	0.190	0.129	0.221	0.059	0.450
H_2O_2	0.115	0.234	0.109	0.086	0.063	0.060	0.882
SO_2	0.007	0.004	0.004	0.004	0.005	0.005	0.166

As in section 4.3, we conducted five sensitivity runs with different ice retention factors (Table 3), and a run without wet scavenging using the new conversion rate of cloud water to rain water. The simulated vertical profiles of the soluble trace gases, mean mixing ratios in the UT outflow region, and SEs are shown in Figure 8, Table 5, and Figure 9,

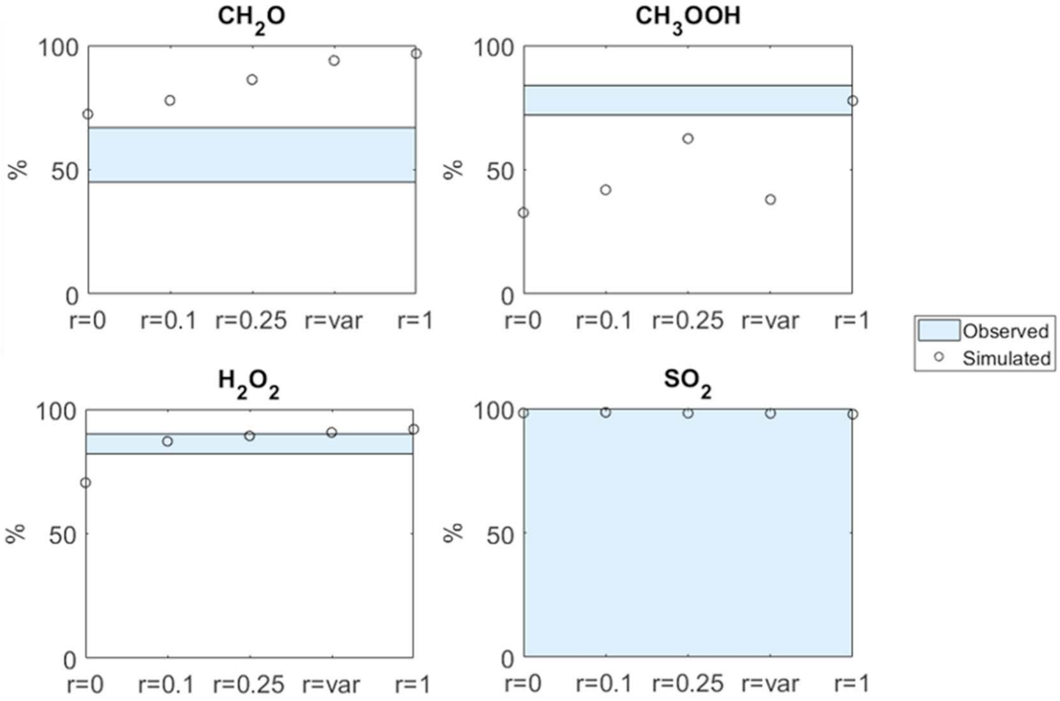

Figure 9. Similar to Figure 6, but for the five sensitivity runs with the new conversion rate of cloud water to rain water.

respectively. Compared to the results in section 4.3, use of the new conversion rate increases the UT CH_2O, CH_3OOH, and H_2O_2 mixing ratios when using the same ice retention factors. From Figure 8 and Table 5, $r = 0$ produced the best result for CH_2O; $r = 0.1–0.25$ produces the best result for CH_3OOH; and $r = 0–0.1$ produces the best result for H_2O_2. All the wet scavenging runs well reproduced the observed SO_2 in UT.

Based on all the mixing ratio vertical profile results in sections 4.3 and 4.4, we conclude that the best estimates of the ice retention factors are $r = 0$ for CH_2O, $r = 0.1–0.25$ for CH_3OOH, and $r = 0–0.1$ for H_2O_2. The model SO_2 results were insensitive to ice retention factor possibly because most SO_2 is removed by liquid phase scavenging due to the high solubility of SO_2. The best estimates of the ice retention factor for CH_2O and H_2O_2 are close to the cloud-resolved results (Bela et al., 2018), which are $r = 0–0.5$ for CH_2O and $r = 0–0.25$ for H_2O_2. However, the result for CH_3OOH is different from the cloud-resolved result (Bela et al., 2016), which is $r = 1$ for CH_3OOH. This is probably because the model performs too much wet scavenging below the freezing level.

5. Summary

In this paper, we evaluated and improved the representation of subgrid wet scavenging of four soluble species (CH_2O, CH_3OOH, H_2O_2, and SO_2) in WRF-Chem. We used WRF-Chem to simulate the 29 May supercell storm observed during the DC3 field campaign at 36-km resolution and compared the modeled and aircraft-measured mixing ratios of CH_2O, CH_3OOH, H_2O_2, and SO_2. Formaldehyde and the peroxides are important HO_x precursors, necessary for O_3 production. SO_2 is the precursor for sulfate aerosol.

Simulation results showed that the default WRF-Chem subgrid wet-scavenging scheme removes too much CH_2O, CH_3OOH, and H_2O_2 in the UT. This could be caused by either the effective solubility of the trace gas when ice and supercooled water are present or the conversion of cloud water to rain or both. Thus, in order to improve the model simulation of subgrid-scale wet scavenging, we added two modifications to the model. The first modification is adjusting the solubility of the tracer by introducing an ice retention factor, and the second modification is changing the conversion rate of cloud water to rain water by using the Han et al. (2016) scheme.

The introduction of the ice retention factor improves the model simulation of CH_2O, CH_3OOH, and H_2O_2, for which the wet SEs were overestimated in the default WRF-Chem run. Compared to the default WRF-Chem results, which are in effect $r = 1$ for all soluble species, the differences between the observed and simulated CH_2O, CH_3OOH, and H_2O_2 were reduced by 24%, 87%, and 77%, respectively. The usage of the new conversion rate of cloud water to rain water provided an additional improvement by increasing UT CH_2O, CH_3OOH, and H_2O_2 mixing ratios when using the same ice retention factors. However, the simulated CH_2O was still much lower (71%) than the observation. The SE analysis demonstrated that all the wet scavenging runs overestimate the SE of CH_2O.

Finally, we conclude that the best results were obtained using the Han et al. (2016) conversion rate of cloud water to rain water and ice retention factor for soluble species of $r = 0$ for CH_2O, $r = 0.1–0.25$ for CH_3OOH, and $r = 0–0.1$ for H_2O_2. The SO_2 simulation did not respond to the change of ice retention factor, so we suggest the value from the laboratory results, which is 0.02 (Leriche et al., 2013).

Ozone in the UT is an important radiative gas, and estimating its production in convective outflows is a crucial aspect of understanding the ozone source in the UT. Because HO_x precursors play an important role in producing O_3, representing their convective transport is key. Our study finds that subgrid-scale convective schemes should include ice physics and subgrid-scale wet-scavenging schemes should represent retention of soluble trace gases in ice particles. Further, research should address these issues in other types of storms to determine the robustness of our findings. Moreover, the ice retention factors should be included in subgrid convective transport and wet-scavenging schemes within other regional and global chemical transport models.

Acknowledgments
This work was supported under NSF Grant AGS-1522551 for analysis and modeling associated with the Deep Convective Clouds and Chemistry (DC3) field campaign. M. Bela was supported by NASA ACCDAM-NNX14AR56G and a National Research Council Research Associateship in the Global Systems Division (GSD) at NOAA-ESRL. K. Cummings was employed by NASA through the NASA Pathways Program during completion of this research. We thank the NCAR Computational Systems Laboratory (CISL) for usage of the Yellowstone and Cheyenne supercomputer for conducting the storm simulations. NCAR is operated by the University Corporation for Atmospheric Research under the sponsorship of the National Science Foundation. We extend our appreciation to A. Fried, B. Heikes, P. Wennberg, R. Cohen, and G. Huey for the airborne observations of trace gases used in this analysis. We would like to thank C. R. Homeyer who provided us the NEXRAD data and E. Bruning who provided the lightning flash channel length data from the Oklahoma Lightning Mapping Array. We thank Georg Grell, Saulo Freitas, and Xin-Zhong Liang for helpful discussions. The DC3-merged aircraft data are available at NASA Data Repository website (https://www-air.larc.nasa.gov/cgi-bin/ArcView/dc3-seac4rs). NCEP stage IV precipitation analysis is available at the NCEP website (http://www.emc.ncep.noaa.gov/mmb/ylin/pcpanl/stage4/). NAM-ANL is available at the NOAA National Operational Model Archive and Distribution System website (http://nomads.ncdc.noaa.gov/data/namanl/). MOZART-4 global model output is available online (at http://www.acom.ucar.edu/wrf-chem/mozart.shtml).

References

Anderson, D. C., Loughner, C. P., Diskin, G., Weinheimer, A., Canty, T. P., Salawitch, R. J., et al. (2014). Measured and modeled CO and NO_y in DISCOVER-AQ: An evaluation of emissions and chemistry over the eastern US. *Atmospheric Environment*, *96*, 78–87. https://doi.org/10.1016/j.atmosenv.2014.07.004

Barth, M. C., Bela, M. M., Fried, A., Wennberg, P. O., Crounse, J. D., Clair, J. M. S., et al. (2016). Convective transport and scavenging of peroxides by thunderstorms observed over the central U.S. during DC3. *Journal of Geophysical Research: Atmospheres*, *121*, 4272–4295. https://doi.org/10.1002/2015JD024570

Barth, M. C., Cantrell, C. A., Brune, W. H., Rutledge, S. A., Crawford, J. H., Huntrieser, H., et al. (2015). The Deep Convective Clouds and Chemistry (DC3) field campaign. *Bulletin of the American Meteorological Society*, *96*(8), 1281–1309. https://doi.org/10.1175/BAMS-D-13-00290.1

Barth, M. C., Kim, S.-W., Skamarock, W. C., Stuart, A. L., Pickering, K. E., & Ott, L. E. (2007). Simulations of the redistribution of formaldehyde, formic acid, and peroxides in the 10 July 1996 Stratospheric-Tropospheric Experiment: Radiation, aerosols, and ozone deep convection storm. *Journal of Geophysical Research*, *112*, D13310. https://doi.org/10.1029/2006JD008046

Barth, M. C., Kim, S. -W., Wang, C., Pickering, K. E., Ott, L. E., Stenchikov, G., et al. (2007). Cloud-scale model intercomparison of chemical constituent transport in deep convection. *Atmospheric Chemistry and Physics*, *7*(18), 4709–4731. https://doi.org/10.5194/acp-7-4709-2007

Barth, M. C., Stuart, A. L., & Skamarock, W. C. (2001). Numerical simulations of the July 10, 1996, stratospheric-tropospheric experiment: Radiation, aerosols, and ozone (STERAO)-deep convection experiment storm: Redistribution of soluble tracers. *Journal of Geophysical Research.*, *106*(D12), 12,381–12,400. https://doi.org/10.1029/2001JD900139

Baughcum, S. L., Begin, J. J., Franco, F., Greene, D. L., Lee, D. S., McLaren, M., et al. (1999). Aircraft emissions: Current inventories and future scenarios. Retrieved from https://repository.upenn.edu/library_papers/59

Bela, M. M., Barth, M. C., Toon, O. B., Fried, A., Homeyer, C. R., Morrison, H., et al. (2016). Wet scavenging of soluble gases in DC3 deep convective storms using WRF-Chem simulations and aircraft observations. *Journal of Geophysical Research: Atmospheres*, *121*, 4233–4257. https://doi.org/10.1002/2015JD024623

Bela, M. M., Barth, M. C., Toon, O. B., Fried, A., Ziegler, C., Cummings, K. A., et al. (2018). Effects of scavenging, entrainment, and aqueous chemistry on peroxides and formaldehyde in deep convective outflow over the central and Southeast United States. *Journal of Geophysical Research: Atmospheres*, *123*, 7594–7614. https://doi.org/10.1029/2018JD028271

Carlton, A. G., Turpin, B. J., Altieri, K. E., Seitzinger, S., Reff, A., Lim, H.-J., & Ervens, B. (2007). Atmospheric oxalic acid and SOA production from glyoxal: Results of aqueous photooxidation experiments. *Atmospheric Environment*, *41*(35), 7588–7602. https://doi.org/10.1016/j.atmosenv.2007.05.035

Chameides, W. L. (1984). The photochemistry of a remote marine stratiform cloud. *Journal of Geophysical Research*, *89*(D3), 4739–4755. https://doi.org/10.1029/JD089iD03p04739

Chatfield, R. B., & Crutzen, P. J. (1984). Sulfur dioxide in remote oceanic air: Cloud transport of reactive precursors. *Journal of Geophysical Research*, *89*(D5), 7111–7132. https://doi.org/10.1029/JD089iD05p07111

Crutzen, P. J., & Gidel, L. T. (1983). A two-dimensional photochemical model of the atmosphere: 2. The tropospheric budgets of the anthropogenic chlorocarbons CO, CH_4, CH_3Cl and the effect of various NO_x sources on tropospheric ozone. *Journal of Geophysical Research*, *88*(C11), 6641–6661. https://doi.org/10.1029/JC088iC11p06641

Cummings, K. A. (2017). *An investigation of the parameterized prediction of lightning in cloud-resolved convection and the resulting chemistry, (doctoral dissertation)*. Retrieved from DRUM. College Park, MD: University of Maryland. http://hdl.handle.net/1903/19920

Dickerson, R. R., Huffman, G. J., Luke, W. T., Nunnermacker, L. J., Pickering, K. E., Leslie, A. C. D., et al. (1987). Thunderstorms: An important mechanism in the transport of air pollutants. *Science*, *235*(4787), 460–465. https://doi.org/10.1126/science.235.4787.460

DiGangi, E. A., MacGorman, D. R., Ziegler, C. L., Betten, D., Biggerstaff, M., Bowlan, M., & Potvin, C. K. (2016). An overview of the 29 May 2012 Kingfisher supercell during DC3. *Journal of Geophysical Research: Atmosphere*, *121*, 14,316–14,343. https://doi.org/10.1002/2016JD025690

Fast, J. D., Gustafson, W. I., Easter, R. C., Zaveri, R. A., Barnard, J. C., Chapman, E. G., et al. (2006). Evolution of ozone, particulates, and aerosol direct radiative forcing in the vicinity of Houston using a fully coupled meteorology-chemistry-aerosol model. *Journal of Geophysical Research*, *111*, D21305. https://doi.org/10.1029/2005JD006721

Fried, A., Barth, M. C., Bela, M., Weibring, P., Richter, D., Walega, J., et al. (2016). Convective transport of formaldehyde to the upper troposphere and lower stratosphere and associated scavenging in thunderstorms over the central United States during the 2012 DC3 study. *Journal of Geophysical Research: Atmospheres*, *121*, 7430–7460. https://doi.org/10.1002/2015JD024477

Grassian, V. H. (2005). *Environmental catalysis*. Boca Raton, FL: CRC Press. https://doi.org/10.1201/9781420027679

Grell, G. A., & Freitas, S. R. (2014). A scale and aerosol aware stochastic convective parameterization for weather and air quality modeling. *Atmospheric Chemistry and Physics*, *14*(10), 5233–5250. https://doi.org/10.5194/acp-14-5233-2014

Grell, G. A., Peckham, S. E., Schmitz, R., McKeen, S. A., Frost, G., Skamarock, W. C., & Eder, B. (2005). Fully coupled “online” chemistry within the WRF model. *Atmospheric Environment*, *39*(37), 6957–6975. https://doi.org/10.1016/j.atmosenv.2005.04.027

Guenther, A., Karl, T., Harley, P., Wiedinmyer, C., Palmer, P. I., & Geron, C. (2006). Estimates of global terrestrial isoprene emissions using MEGAN (Model of Emissions of Gases and Aerosols from Nature). *Atmospheric Chemistry and Physics*, *6*(11), 3181–3210. https://doi.org/10.5194/acp-6-3181-2006

Han, J.-Y., Hong, S.-Y., Sunny Lim, K.-S., & Han, J. (2016). Sensitivity of a cumulus parameterization scheme to precipitation production representation and its impact on a heavy rain event over Korea. *Monthly Weather Review*, *144*(6), 2125–2135. https://doi.org/10.1175/MWR-D-15-0255.1

Homeyer, C. R., Pan, L. L., Dorsi, S. W., Avallone, L. M., Weinheimer, A. J., O'Brien, A. S., et al. (2014). Convective transport of water vapor into the lower stratosphere observed during double-tropopause events. *Journal of Geophysical Research: Atmospheres*, *119*, 10,941–10,958. https://doi.org/10.1002/2014JD021485

Iacono, M. J., Delamere, J. S., Mlawer, E. J., Shephard, M. W., Clough, S. A., & Collins, W. D. (2008). Radiative forcing by long-lived greenhouse gases: Calculations with the AER radiative transfer models. *Journal of Geophysical Research*, *113*, D13103. https://doi.org/10.1029/2008JD009944

Iribarne, J. V., & Pyshnov, T. (1990). The effect of freezing on the composition of supercooled droplets—I. Retention of HCl, HNO3, NH3 and H2O2. *Atmospheric Environment. Part A. General Topics*, *24*(2), 383–387. https://doi.org/10.1016/0960-1686(90)90118-7

Iribarne, J. V., Pyshnov, T., & Naik, B. (1990). The effect of freezing on the composition of supercooled droplets—II. Retention of S (IV). *Atmospheric Environment. Part A. General Topics*, *24*(2), 389–398. https://doi.org/10.1016/0960-1686(90)90119-8

Janjić, Z. I. (1994). The Step-Mountain Eta Coordinate Model: Further developments of the convection, viscous sublayer, and turbulence closure schemes. *Monthly Weather Review*, *122*(5), 927–945. https://doi.org/10.1175/1520-0493(1994)122<0927:TSMECM>2.0.CO;2

Jost, A., Szakáll, M., Diehl, K., Mitra, S. K., & Borrmann, S. (2017). Chemistry of riming: The retention of organic and inorganic atmospheric trace constituents. *Atmospheric Chemistry and Physics*, *17*(16), 9717–9732. https://doi.org/10.5194/acp-17-9717-2017

Kong, F., & Qin, Y. (1993). The vertical transport of air pollutants by convective clouds. Part I: A non-reactive cloud transport model. *Advances in Atmospheric Sciences*, *10*, 415–427.

Kong, F., & Qin, Y. (1994). The vertical transport of air pollutants by convective clouds. Part II: Transport of soluble gases and sensitivity tests. *Advances in Atmospheric Sciences*, *11*, 1–12.

Koren, V., Schaake, J., Mitchell, K., Duan, Q.-Y., Chen, F., & Baker, J. M. (1999). A parameterization of snowpack and frozen ground intended for NCEP weather and climate models. *Journal of Geophysical Research*, *104*(D16), 19,569–19,585. https://doi.org/10.1029/1999JD900232

Lacis, A. A., Wuebbles, D. J., & Logan, J. A. (1990). Radiative forcing of climate by changes in the vertical distribution of ozone. *Journal of Geophysical Research*, *95*(D7), 9971–9981. https://doi.org/10.1029/JD095iD07p09971

Lawrence, M. G., & Crutzen, P. J. (1998). The impact of cloud particle gravitational settling on soluble trace gas distributions. *Tellus B*, *50*(3), 263–289. https://doi.org/10.3402/tellusb.v50i3.16129

Leriche, M., Pinty, J.-P., Mari, C., & Gazen, D. (2013). A cloud chemistry module for the 3-D cloud-resolving mesoscale model Meso-NH with application to idealized cases. *Geoscientific Model Development*, *6*(4), 1275–1298. https://doi.org/10.5194/gmd-6-1275-2013

Li, Y., Pickering, K. E., Allen, D. J., Barth, M. C., Bela, M. M., Cummings, K. A., et al. (2017). Evaluation of deep convective transport in storms from different convective regimes during the DC3 field campaign using WRF-Chem with lightning data assimilation. *Journal of Geophysical Research: Atmospheres*, *122*, 7140–7163. https://doi.org/10.1002/2017JD026461

Li, Y., Pickering, K. E., Barth, M. C., Bela, M. M., Cummings, K. A., & Allen, D. J. (2018). Evaluation of parameterized convective transport of trace gases in simulation of storms observed during the DC3 field campaign. *Journal of Geophysical Research: Atmospheres*, *123*, 11,238–11,261. https://doi.org/10.1029/2018JD028779

Lim, K.-S. S. (2011). *Investigation of aerosol indirect effects on simulated moist convections*. Ph.D. dissertation. Seoul, South Korea, 186: Yonsei University.

Lyons, W. A., Calby, R. H., & Keen, C. S. (1986). The impact of mesoscale convective systems on regional visibility and oxidant distributions during persistent elevated pollution episodes. *Journal of Climate and Applied Meteorology*, *25*(11), 1518–1531. https://doi.org/10.1175/1520-0450(1986)025<1518:TIOMCS>2.0.CO;2

Mari, M., Cembali, T., Casalini, L., & Pratella, G. C. (2000). Mucor species in orchard soil-population dynamics and pathogenicity on pear fruit. *European Journal of Plant Pathology*, *106*(5), 449–454. https://doi.org/10.1023/A:1008751328500

Morrison, H., Thompson, G., & Tatarskii, V. (2009). Impact of cloud microphysics on the development of trailing Stratiform precipitation in a simulated squall line: Comparison of one- and two-moment schemes. *Monthly Weather Review*, *137*(3), 991–1007. https://doi.org/10.1175/2008MWR2556.1

Neu, J. L., & Prather, M. J. (2012). Toward a more physical representation of precipitation scavenging in global chemistry models: Cloud overlap and ice physics and their impact on tropospheric ozone. *Atmospheric Chemistry and Physics*, *12*(7), 3289–3310. https://doi.org/10.5194/acp-12-3289-2012

Ott, L. E., Bacmeister, J., Pawson, S., Pickering, K., Stenchikov, G., Suarez, M., et al. (2009). Analysis of convective transport and parameter sensitivity in a single column version of the Goddard Earth Observation System, version 5, general circulation model. *Journal of the Atmospheric Sciences*, *66*(3), 627–646. https://doi.org/10.1175/2008JAS2694.1

Pfister, G. G., Avise, J., Wiedinmyer, C., Edwards, D. P., Emmons, L. K., Diskin, G. D., et al. (2011). CO source contribution analysis for California during ARCTAS-CARB. *Atmospheric Chemistry and Physics*, *11*(15), 7515–7532. https://doi.org/10.5194/acp-11-7515-2011

Pickering, K. E., Scala, J. R., Thompson, A. M., Tao, W.-K., & Simpson, J. (1992). A regional estimate of convective transport of CO from biomass burning. *Geophysical Research Letters*, *19*(3), 289–292. https://doi.org/10.1029/92GL00036

Pickering, K. E., Thompson, A. M., Dickerson, R. R., Luke, W. T., McNamara, D. P., Greenberg, J. P., & Zimmerman, P. R. (1990). Model calculations of tropospheric ozone production potential following observed convective events. *Journal of Geophysical Research*, *95*(D9), 14,049–14,062. https://doi.org/10.1029/JD095iD09p14049

Pickering, K. E., Thompson, A. M., Kim, H., DeCaria, A. J., Pfister, L., Kucsera, T. L., et al. (2001). Trace gas transport and scavenging in PEMTropics B South Pacific Convergence Zone convection. *Journal of Geophysical Research*, *106*(D23), 32,591–32,607. https://doi.org/10.1029/2001JD000328

Pickering, K. E., Thompson, A. M., Scala, J. R., Tao, W.-K., Dickerson, R. R., & Simpson, J. (1992). Free tropospheric ozone production following entrainment of urban plumes into deep convection. *Journal of Geophysical Research*, *97*(D16), 17,985–18,000. https://doi.org/10.1029/92JD01716

Prather, M. J., & Jacob, D. J. (1997). A persistent imbalance in HO_x and NO_x photochemistry of the upper troposphere driven by deep tropical convection. *Geophysical Research Letters*, *24*(24), 3189–3192. https://doi.org/10.1029/97GL03027

Price, C., & Rind, D. (1992). A simple lightning parameterization for calculating global lightning distributions. *Journal of Geophysical Research*, *97*(D9), 9919–9933. https://doi.org/10.1029/92JD00719

Qiao, F., & Liang, X.-Z. (2015). Effects of cumulus parameterizations on predictions of summer flood in the Central United States. *Climate Dynamics*, *45*(3-4), 727–744. https://doi.org/10.1007/s00382-014-2301-7

Qiao, F., & Liang, X.-Z. (2016). Effects of cumulus parameterization closures on simulations of summer precipitation over the United States coastal oceans. *Journal of Advances in Modeling Earth Systems*, *8*, 764–785. https://doi.org/10.1002/2015MS000621

Qiao, F., & Liang, X.-Z. (2017). Effects of cumulus parameterization closures on simulations of summer precipitation over the continental United States. *Climate Dynamics*, *49*(1-2), 225–247. https://doi.org/10.1007/s00382-016-3338-6

Skamarock, W. C., & Klemp, J. B. (2008). A time-split nonhydrostatic atmospheric model for Weather Research and Forecasting applications. *Journal of Computational Physics*, *227*(7), 3465–3485. https://doi.org/10.1016/j.jcp.2007.01.037

Skamarock, W. C., Powers, J. G., Barth, M., Dye, J. E., Matejka, T., Bartels, D., et al. (2000). Numerical simulations of the July 10 stratospheric tropospheric experiment: Radiation, aerosols, and ozone/deep convection experiment convective system—Kinematics and transport. *Journal of Geophysical Research*, *105*(D15), 19,973–19,990. https://doi.org/10.1029/2000JD900179

Snider, J. R., & Jun, H. (1998). Factors influencing the retention of hydrogen peroxide and molecular oxygen in rime ice. *Journal of Geophysical Research*, *103*(D1), 1405–1415. https://doi.org/10.1029/97JD02847

Solomon, S., Rosenlof, K. H., Portmann, R. W., Daniel, J. S., Davis, S. M., Sanford, T. J., & Plattner, G.-K. (2010). Contributions of stratospheric water vapor to decadal changes in the rate of global warming. *Science*, *327*(5970), 1219–1223. https://doi.org/10.1126/science.1182488

Tie, X., Madronich, S., Walters, S., Zhang, R., Rasch, P., & Collins, W. (2003). Effect of clouds on photolysis and oxidants in the troposphere. *Journal of Geophysical Research*, *108*(D20), 4642. https://doi.org/10.1029/2003JD003659

Travis, K. R., Jacob, D. J., Fisher, J. A., Kim, P. S., Marais, E. A., Zhu, L., et al. (2016). Why do models overestimate surface ozone in the Southeast United States? *Atmospheric Chemistry and Physics*, *16*(21), 13,561–13,577. https://doi.org/10.5194/acp-16-13561-2016

von Blohn, N., Diehl, K., Mitra, S. K., & Borrmann, S. (2011). Wind tunnel experiments on the retention of trace gases during riming: Nitric acid, hydrochloric acid, and hydrogen peroxide. *Atmospheric Chemistry and Physics*, *11*(22), 11,569–11,579. https://doi.org/10.5194/acp-11-11569-2011

Wiedinmyer, C., Akagi, S. K., Yokelson, R. J., Emmons, L. K., Al-Saadi, J. A., Orlando, J. J., & Soja, A. J. (2011). The Fire INventory from NCAR (FINN): A high resolution global model to estimate the emissions from open burning. *Geoscientific Model Development*, *4*(3), 625–641. https://doi.org/10.5194/gmd-4-625-2011

Wong, J., Barth, M. C., & Noone, D. (2013). Evaluating a lightning parameterization based on cloud-top height for mesoscale numerical model simulations. *Geoscientific Model Development*, *6*(2), 429–443. https://doi.org/10.5194/gmd-6-429-2013